Introduction

I.1 Active Galactic Nuclei

Active Galactic Nuclei (hereafter AGN) appear as bright point sources located in the center of galaxies. In galaxies hosting an AGN (at least 17% of galaxies in optical spectroscopic surveys, Ho et al. 1997, Carter et al. 2001, Miller et al. 2003) the luminosity of the point-like nucleus ($10^{44}-10^{46}$ erg s^{-1}) always dominates over the starlight luminosity of the entire galaxy by at least an order of magnitude.
The emission of radiation from AGN covers the entire electromagnetic spectrum, from radio to gamma-ray energies. It is understood that the primary source of energy empowering this enormous release of radiation is the gravitational infall of matter onto a supermassive black hole (hereafter SMBH), with a mass ranging from 10^6 up to a few 10^9 $M_\odot$. This is in fact the most efficient way in nature of extracting energy from matter. For instance, in the case of gravitational accretion onto a fast rotating black hole, the rate of conversion of matter into energy can be up to ∼30% (e.g., Bambi 2012). For comparison, the efficiency of nuclear fusion of hydrogen is only ∼0.7%.
The AGN taxonomy is wide. For historical reasons, local AGN (at redshift z$\lesssim$0.1) are referred to as "Seyfert" galaxies, while more luminous (with a bolometric luminosity $L_{\rm bol} \gtrsim 10^{45}$erg s^{-1}) and distant AGN are more often named as quasars. In the optical AGN are divided into two main classes. The so-called type 1 AGN show broad (BL, with a full width at half maximum *FWHM*$\geq$ 1000 km s^{-1}) and narrow (NL, *FWHM*$\leq$500 km s^{-1}) emission lines in their spectrum, while in type 2 AGN, only NL are present (e.g., Netzer 1990). About ∼15–20% of quasars are ∼100 times brighter at radio than at optical wavelengths (Kellermann et al. 1989). Differently from most radio-quiet AGN, these radio-loud AGN show ∼kpc extended lobe of radio emission (e.g., Centaurus A, Israel 1998).
In the '90s a simple explanation that unified AGN phenomenology was put forward. This so-called "Unified Model" (Fig. I.1 Antonucci 1993, Urry & Padovani 1995) in its basic prescription is still valid today. We give here a brief overview of the basic features of the Unified Model, while in Sect. I.1.1–Sect I.1.5 we summarize in detail the different regions of the AGN.
It is believed that the matter falling onto the SMBH forms a thin accretion disk around it, which emits thermal radiation mostly at optical/UV wavelengths. In the innermost AGN region, close to the SMBH, resides a corona of hot electrons, which Compton upscatters the disk radiation to X-ray wavelengths. The UV-to-X-ray radiation produced in the nuclear region photoionizes the ambient gas. The circumnuclear ionized gas is thought to be distributed in two main regions. The fast moving gas in the so-called Broad Line Region (BLR), which is located in the vicinity of the nucleus is thought to produce the BL. On the other hand, the gas producing the NL is distributed in a roughly conical

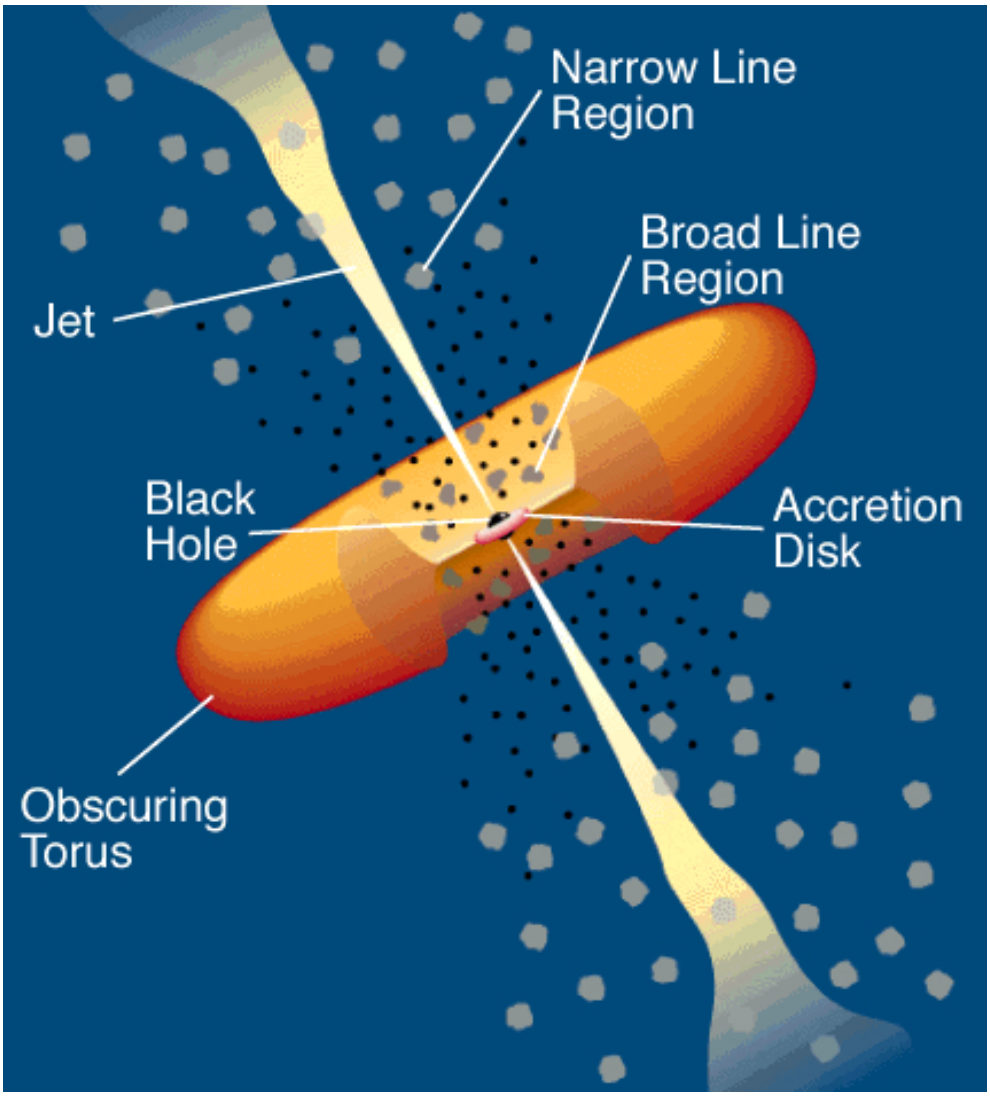

Figure I.1: Sketch of the standard Unified Model for AGN, not to scale. The different AGN regions are labeled. The presence of an optically-thick torus determines an anisotropic obscuration of the nuclear region. From Urry & Padovani (1995).

Narrow Line Region (NLR) located farther from nucleus. The key ingredient of the Unified Model is an optically-thick torus, which prevents a direct view of the nucleus and of the BLR to equatorial observers. In this framework, the type 1/ type 2 bimodality is readily explained as an orientation effect. Namely, type 1 AGN will be those which are viewed

from a polar line of sight that does not intercept the obscuring torus. In radio-loud AGN the radio emission is due to a collimated jet of relativistic electrons that emits synchrotron radiation. The jet is absent in radio-quiet AGN.
This general picture of AGN anatomy is supported by solid observational evidence. For instance, the idea that an accretion disk surrounding a SMBH is present in AGN is strongly supported by the observations of relativistically broadened iron emission line in AGN X-ray spectra (see Reynolds & Nowak 2003, for a review). The line is thought to be produced by reflection (i.e. back-scattering) of the X-ray radiation coming from the hot corona near the disk. The observed line profile (e.g. in the prototypical case of MCG-6-30-15, Tanaka et al. 1995) is explained if both the relativistic Doppler distortion due to the orbital motion of the disk material around the black hole, and the gravitational redshift of the SMBH field (i.e. "clocks near black holes run slowlier") are considered.
A proof that the BLR gas is orbiting in the gravitational field produced by a SMBH is offered, for instance, by the so-called reverberation mapping (Peterson & Horne 2004). This consists in measuring the time delay after which a BL responds to changes of the optical/UV continuum. If interpreted as light-travel time ($\tau_{\rm LT} \sim r/c$, where c is the speed of light), this delay is a measure of the radius r at which the line is produced. This allows to directly measure the mass M of the SMBH assuming that the line width ΔV is simply due to Keplerian motion ($\Delta V^2 \sim M/r$).
Finally, a quite convincing evidence in favor of the Unified Model has been the discovery of polarized broad emission lines in e.g., the prototypical Seyfert 2 NGC 1068 (Antonucci & Miller 1985). This indicates that, although not visible, a BLR is still present in obscured AGN. The optical polarization of type 2 AGN, being perpendicular to the main source axis, is explained if the radiation coming from the BLR is scattered in our line of sight by free electrons located in a conical region along the pole of an obscuring torus coaxial with the source. Indeed, in this configuration, the torus prevents a direct view of the nuclear region and, at the same time suppresses the scattered light in a significant range of angles.

I.1.1 The accretion disk

The matter falling onto the central SMBH, before disappearing beyond the event horizon, orbits around it and forms an accretion disk. The inner radius of the disk $R_{\rm in}$ is nominally set by the radius of the innermost stable circular orbit ($R_{\rm ISCO}$) of a test particle in the space-time metric around the black hole. Thus, ultimately, it depends on the black hole mass M and on its spin (Carter 1971). The same holds for the accretion efficiency $\eta = L_{\rm bol}/\dot{M}\,c^2$ (where $L_{\rm bol}$ is the bolometric luminosity of the disk and $\dot{M}$ is the mass accretion rate).
Theoretical calculations in a general relativity framework predict that the accretion disk around a classical, non rotating, Schwarzschild black hole starts at $6R_{\rm g}$ (where $R_{\rm g} = GM/c^2$ is the gravitational radius) and has an efficiency $\eta = 0.057$. When the black hole spin is included in the computation the Kerr metric has to be used. For a rotating Kerr black hole, $R_{\rm ISCO}$ decreases steeply as the spin increases, while the efficiency increases. For an asymptotic, maximally rotating black hole $R_{\rm in} = 1R_{\rm g}$ and $\eta = 0.42$ (e.g., Bambi 2012).
For a typical AGN hosting a black hole of 10^8 $M_\odot$, $R_{\rm g}$ is of the order 10^{-5} pc, which means

that the inner radius of the disk lies at a distance of a fraction of light hours from the black hole. At large radii the disk self gravity becomes important and the disk is unstable to self-fragmentation (Toomre 1964). This self-fragmentation radius, which is of the order $\sim 10^4\, R_g = 0.1$ pc for a black hole mass 10^8 $M_\odot$, nominally defines the outer boundary of the disk.

At first approximation, the spectrum emitted by the accretion disk is modeled well by the classical Shakura-Sunyaev model of a geometrically-thin, optically-thick disk (Shakura 1973). This ideal disk emits a blackbody-like spectrum which is obtained by integrating the blackbody spectrum of a thin disk annulus over the radial temperature profile of the disk. The latter scales with the black hole mass as $M^{-1/4}$, which means that disks around lighter black holes are hotter and emit at shorter wavelengths (see e.g., Peterson 1997). For instance, the accretion disk around $\sim 10^8$ $M_\odot$black hole radiates predominantly in the far UV part of the spectrum, while for $\sim 10^6$ $M_\odot$black hole the peak of emission is in the extreme UV. Conversely, for stellar-mass black hole of few $M_\odot$, the peak of the disk emission is in the X-ray band.

I.1.2 The hot corona

The blackbody emission of the disk declines towards X-ray energies. The X-rays at energies above ∼2.0 keV are thought to originate in a hot tenuous plasma which probably resides in the inner part of the accretion flow (Haardt & Maraschi 1991). The X-ray emission is produced via inverse Compton scattering of the disk-photons by the hot electrons of this corona. The resulting X-ray spectrum has a power-law shape with an exponential cutoff at high energies. The electron temperature of the corona (kT=20–100 keV) can be directly obtained by simultaneously measuring the slope and the high energy cutoff of the hard X-ray power law (see Malizia et al. 2014). On the other hand, observationally probing the location and the geometry of the X-ray emitting region is challenging (but see Reis & Miller 2013, and references therein). Recent results of X-ray spectral-timing analysis of AGN set the distance between the corona and the accretion disk to be in the 1–10 R_g range. Moreover, the rapid variability of the hard X-ray emission of AGN suggests that the corona is compact in size. Indeed, in a few gravitationally lensed quasars, the size of X-ray emitting region has been measured to be of the order of ∼10 gravitational radii.

I.1.3 The line emitting gas

Emission lines from a variety of ionized species and with a bimodal line width (where the BL have a *FWHM* up to $\sim 10^4$ km s^{-1}and the NL of the order of 10^1 km s^{-1}) are observed across the electromagnetic spectrum of AGN. Broad Balmer hydrogen lines are prominent in the optical spectrum of type 1 AGN (Sulentic et al. 2000), while the UV band covers the transitions from the hydrogen Lyman series (Scott et al. 2004) and from more highly ionized carbon, nitrogen, and oxygen species (e.g., C IV, Bachev et al. 2004). Later, broad lines from e.g., O VII, Ne IX, have were also detected in the X-ray (Costantini et al. 2007, Detmers et al. 2011).

Conversely, NL are present in the spectra of both type 1 and type 2 AGN. In the optical

band, a narrow [O III] $\lambda\lambda$5007, 4959 Å doublet is typically seen. In the UV and in the X-ray spectrum of type 1 AGN NL are often difficult to be disentangled from either the prominent BL or the bright continuum. However, in some cases, a temporary low X-ray continuum allows the detection of a rich spectrum of X-ray NL, of which the O VII forbidden line is usually the most prominent line. (e.g., Whewell et al. 2015).

Photoionization is the most likely source of line excitation for the AGN circumnuclear gas (see Netzer 2008, for a review). A direct evidence in favor of this is, for instance the correlated line and continuum variations observed during reverberation mapping campaigns of Seyfert galaxies. Photoionization equilibrium (i.e. the balance between the ionization and the recombination rate) is reached at temperatures of the order $\sim 10^4$ K for a wide variety of astrophysical plasmas. The temperature of the line-emitting gas in AGN can be directly estimated using the measured ratios of the strengths of emission lines with different upper levels (Osterbrock 1989), such as [O III] [I(λ4959) + I(λ5007)] / I(λ4363). These measurements usually indicate a temperature typical of photoionization for the NLR gas.

Despite being both dominated by photoionization, under other respects the BLR and the NLR are two different gaseous environments. The absence of strong broad forbidden lines indicates that the gas in the BLR must have a density of the order of at least $\sim 10^8$ cm^{-3}. This is the critical density above which the [O III] forbidden line is collisionally suppressed. The geometry, the kinematics and the ionization conditions of the BLR gas can be probed using reverberation mapping techniques and photoionization modeling. The BLR size that is deduced from measurements of reverberation lags of e.g. the H_β line ranges between 10 and 100 light days (Peterson et al. 2004). Interestingly, the inferred BLR size correlates with the AGN optical luminosity as $\sim L_{5100}^{0.7}$ (where L_{5100} is the luminosity at 5100 Å, see Kaspi et al. 2000). This matches qualitatively with what is expected in a photoionization scenario, where the luminosity of the ionizing source regulates the size of the zone of ionized gas. High ionization lines are found to respond to continuum variations faster than low ionization lines, which indicates that the BLR gas is stratified in ionization. The spatial distribution of the line emission in the BLR has been modeled using the LOC (locally optimally emitting cloud, Baldwin et al. 1995) approach. This model is based on the idea that line-emitting clouds of gas of various density are distributed around the nucleus. Emission of a particular line comes predominantly from a location where clouds with optimal conditions for the emission of that line reside. The LOC model has been used to successfully model the optical and UV BLR (Korista et al. 1997, Korista & Goad 2000) and more recently, in a few cases, (e.g. Costantini et al. 2007) it has been extended to the X-ray BL.

In contrast to the BLR, the NLR does exhibit the [O III] forbidden transition which indicates a lower density of the emitting gas ($n = 10^3 - 10^6$ cm^{-3}, see a review from Netzer 1990). Another difference is that the NL are not observed to vary, even in sources undergoing drastic continuum changes. This suggests that the NL are emitted at larger distance from the center and that the NLR itself is spatially extended. Indeed, in nearby Seyfert 2 the NLR is spatially resolved and can be directly imaged (e.g., Circinus, Wilson et al. 2000, NGC 1068, Pogge 1988) . These studies indicate a conical geometry for the NLR gas, extended up to distances of the order of $\sim$100 pc. The NLR is a complex gaseous environment, and

a LOC photoionization modeling is required to account for the observed properties of the optical/UV NLR (Ferguson et al. 1997). Concerning the X-ray NL, Bianchi et al. (2006) found that a density profile scaling like $\sim r^2$ is required to reproduce the observed [O III] to soft X-ray ratio observed in spatially resolved X-ray and optical images of the NLR in nearby Seyfert 2. For a tentative optical-to-X-ray photoionization modeling of the NLR in a nearby quasar see chapter 1.

I.1.4 The obscuring torus

A toroidally-shaped, dusty structure screening the central engine on the equatorial line of sight was firstly invoked in Antonucci (1993) to account for the observed type 1-type 2 AGN bimodality. The toroidal geometry of the obscuring medium was initially inferred from the observed optical polarization of type 2 AGN. The measured polarization angles can be explained by the presence of an absorber preventing the nuclear light to be scattered in a significant range of angles. A torus shape is the simplest configuration which achieves this effect. The observed biconical geometry of the ionized gas in NLR, that is not obscured by the torus, is also naturally explained in this geometrical configuration.
In the context of the Unified Model, the location of the inner edge of the torus, nominally separating it from the BLR, can be set by the dust sublimation radius beyond which dust grains can survive the AGN radiation field. This is ultimately regulated by the AGN luminosity (e.g., Krolik & Kriss 2001). Thus, it is at ∼sub-pc scales in Seyfert objects and at ∼pc scale at quasar luminosities.
Probing the location and the detailed geometry of the obscuring material in AGN is a crucial test for the current theoretical paradigm.
The dust in the torus absorbs the AGN X-ray/UV radiation and re-emits thermally at infrared wavelengths. The K band wavelength (∼2.2μm) is close to the peak emissivity of the hottest dust. Thus, in this band, the reverberation lag technique probes the torus inner boundary (Suganuma et al. 2006, Kishimoto et al. 2007, Koshida et al. 2014, Pozo Nuñez et al. 2014). The time-lags measured in these experiments, which were successfully carried out for a handful of medium-to-low redshift AGN, are a factor 3-4 larger than those found in the optical for e.g. the Hβ broad emission line. This indicates that the BLR is limited in size (Landt et al. 2014) by the inner wall of the torus, which is in good agreement with the Unified Model.
At longer, mid-infrared (MIR) wavelengths (8–13 μm), colder dust can be probed. Recently, thanks to the significant improvements in the long-baseline IR interferometry offered by the ESO MID-infrared interferometric instrument (MIDI, see e.g., Jaffe et al. 2004, Burtscher et al. 2013) and the Astronomical Multi-BEam combiner (AMBER, see e.g., Weigelt et al. 2012), it has become possible to map the distribution the of MIR-emitting dust with an unprecedented spatial resolution of the order of few milliarcseconds. For a few well observed nearby sources, the detailed geometry of the dust emission could be revealed. For instance, Tristram et al. (2014) modeled the emissivity map of Circinus in three MIR bands. Roughly 20% of the MIR flux is emitted by a thin, centrally located, 1 pc large, disk like structure while the bulk (∼80%) of the MIR emission comes from a second, thicker component, elongated along the polar direction. A somewhat similar structure

has been observed also in two other type-2 AGN (NCG 1068 Raban et al. 2009, and NGC 424. Hönig et al. 2012) and in the type-1 source NGC 3783 (Hönig et al. 2013). Moreover, 18 out 123 sources in the Asmus et al. (2016) sample show clear indication of an elongated MIR morphology, and it is argued that this detection rate is artificially lowered by e.g., the lack of sufficient high-quality datasets in the sample.
These findings challenge the simple torus paradigm of the Unified Model. While the hot, NIR-emitting dust may indeed be confined in a central small equatorial torus, much of the cooler dust may reside in an extended region having an elongated geometry and, possibly, a different dynamic (e.g., a wind, as argued in Hönig et al. 2012, 2013).
Indications for a more complex geometrical distribution of the obscuring material in AGN are provided also by studies the X-ray band (see Bianchi et al. 2012, and references therein). Recent results from X-ray variability studies indicate that some cold obscuring material, likely in the form of clumps, is present within the dust sublimation radius also in optically unobscured type 1 AGN (see Sect.I.3.2). These findings are naturally explained in the context of new theoretical models of non-uniform clumpy tori (Elitzur & Shlosman 2006, Nenkova et al. 2008, Hönig & Kishimoto 2010). These models are promising because as well as accounting for the time-variable X-ray obscuration, they also reproduce better the IR SED of both type 1 and the type 2 AGN over the full range of IR wavelengths covered (Nenkova et al. 2002).
In a clumpy torus framework the BLR, and the dusty torus are part of the same clumpy medium which decreases in ionization as the distance from the center increases. In this context, the AGN classification must be reinterpreted. The degree of obscuration is determined not only by the observer's viewing angle, but also by the cloud number density on the equatorial plane. When the cloud number density is low, the source may appear as an unobscured type 1 AGN even to equatorial observers.
All in all, while the classical model of a uniform axysimmetric torus has been proven to be inadequate by these, and others pieces of evidence, a new paradigm is far from being firmly set (see Netzer 2015, and references therein). The nature of the AGN obscurer remain uncertain and a comprehensive picture of how it forms, evolves and remains stable over a long period of time is still missing.

I.1.5 The relativistic jet

The synchrotron radio emission from a jet distinguishes radio-loud from radio-quiet AGN. Radio-quiet AGN are not always radio-silent, as in some cases they show evidence for weaker radio lobes (Panessa et al. 2014). For an overview of the observational properties of AGN jets see Hardee (2008). For the purpose of this thesis, it is important to clarify the difference between AGN jets and winds (see e.g., Königl 2006). A jet is a highly-collimated flow of relativistic particles, which emits non-thermal radiation. On the other hand, winds are less collimated flow of ionized gas, identified by their thermal emission signatures. The outflow velocity of a wind, even for the fastest cases, is always sub-relativistic ($v_{\rm out} \leq 0.1c$).

I.2 Rationale of this thesis

The Unified Model has been an ambitious attempt of explaining a vast observational taxonomy using a small number of physical parameters. Namely, the source inclination with respect of the observer line of sight determine the detectability of the nucleus and of the optical/UV/X-ray BLR, while the presence (or the absence) of a jet determine the AGN radio-loudness (or quietness). Undoubtedly, this model has enabled a significant progress in our understanding of the AGN phenomenon. Nevertheless, some questions remain open (see e.g., Beckmann & Shrader 2012).
In this thesis we use X-ray spectroscopy to characterize the central engine and the circumnuclear environment in some nearby AGN. Using high-resolution X-ray spectroscopy, it is possible to probe the physical conditions in the absorbing/emitting photoionized gas surrounding the black hole. This ionized material is often found to be part of a fast outflow. As we shall see, AGN winds are theoretically expected to have a profound impact on the surrounding galactic environment. For this reason, the possible impact of winds beyond the AGN boundary is currently a matter of investigation in observational astrophysics.

I.2.1 The role of winds in shaping the AGN environment

A potentially crucial additional ingredient in the AGN science is a wind energized by the black hole activity and interacting with the interstellar medium of the host galaxy.
From a theoretical point of view there are reasons to expect an important wind component in AGN. For instance, accretion disk winds of various kinds have been invoked in models for the formation of the jet (e.g., Blandford & Payne 1982) and of the torus clumpy medium (e.g., Elitzur & Shlosman 2006). It is also straightforward to prove that the AGN activity must somehow regulate the star-formation in the host galaxy. Indeed, a tight correlation between the mass of the central black hole and the stellar mass of the galactic bulge (the so-called M-σ relation, Merritt & Ferrarese 2001) holds. This relation naturally follows as a consequence of the so-called AGN feedback scenario. Detailed numerical simulations of the galaxy/black hole coevolution (Di Matteo et al. 2005, Scannapieco & Oh 2004, Sijacki et al. 2007, Hopkins et al. 2008, Hopkins & Elvis 2010) show that the energy output from the accreting SMBH results in powerful gas outflows. These winds effectively deplete the galaxy of its cold gas, thereby halting the star formation and preventing further black hole growth.
An accretion disk around a black hole can launch a wind, provided that either the gradient of gas pressure (thermal driving), or the radiation force (radiative driving) or the Lorentz force (magnetic driving) overcomes the gravitational force (see Proga 2007, for a review). Radiatively and magnetically driven disk winds are theoretically expected to reach the highest terminal velocities, of the order 10^4 km s^{-1} (Proga et al. 2000, Everett 2005). Fast disk winds are able to drive a large-scale outflow in the ISM of the host galaxy provided that energy is conserved in the wind-ISM interaction, i.e., that the shocked hot ISM does not radiatively cool on a timescale shorter than its flow time (King & Pounds 2015, and references therein). The large-scale outflow is able to clear up a galaxy of its gas as required in the AGN feedback scenario.

Outflows of different kinds are observed across the electromagnetic spectrum of AGN, from X-ray to radio wavelengths. Observations in different bands probe outflows in different phases, from the highly-ionized gas to the cold, molecular, gas. However, so far, observations of AGN outflows have not yet provided a firm confirmation of the AGN feedback scenario, nor have allowed to definitively discriminate between different wind driving mechanisms.

In the X-rays two classes of highly-ionized gas outflow are probed. The so-called ultrafast outflows (UFO) are highlighted by blueshifted absorption lines from the most highly-ionized iron species (Fe XXV–Fe XXVI). These highly-ionized winds reach mildly relativistic velocities (of the order ∼0.1 c) and are believed to be accelerated out of the accretion disk, possibly via magnetic driving (Tombesi et al. 2012). Conversely, the so-called warm absorbers (WA, see Sect. I.4 for a detailed description) can be detected in both the X-ray and the UV band via narrow absorption lines (NAL) of several ionized species of e.g., Fe, Si, Mg, O, N, and, C. These are more gentle winds reaching velocities of the order of few thousands km s^{-1}.

An interesting class of AGN showing outflows in the optical/UV band are the so-called broad-absorption line quasars (BAL QSO, see Hamann & Sabra 2004 for a review). These sources display broad (with a typical width of 10^4 km s^{-1}) absorption troughs due to resonant transitions of ionized metals e.g., C IV, N V, O VI, Si IV, which are strongly blueshifted (from few 1000 to few 10 000 km s^{-1}) with respect to the source systemic velocity. Interestingly, in some cases the X-ray spectrum of BAL QSO requires a partially covering or ionized X-ray absorption, which can be variable on timescales as short as few hours. These UV/X-ray properties are consistent with the picture of a nuclear wind (e.g., Giustini et al. 2015).

At optical wavelengths, large scale (∼ kpc, Harrison et al. 2014) galactic winds are revealed. Indicators in the optical band can probe the mildly-ionized, neutral, and dusty component of galactic outflows (Rupke & Veilleux 2013). These winds can in principle be driven by the stellar winds and supernovae generated in a powerful starburst or by the AGN activity or by a combination of the two. However, the high-velocity winds observed in QSO hosts (up to few thousands km s^{-1}) are difficult to be produced from a starburst alone (Rupke & Veilleux 2013).

In the infrared and in the submilimeter, transitions from a plethora of molecular species (e.g., OH, Sturm et al. 2011 and CO, Cicone et al. 2014) highlight massive outflows of cold, molecular gas. This phase of the outflow carries the largest amount of mass away from the galaxy and thus provide the most effective feedback. For instance, in the best-studied case of Mrk 231, the giant molecular outflow seen in CO (Feruglio et al. 2010), OH (Fischer et al. 2010), HCN, HCO+, HNC (Aalto et al. 2012), and, water vapor (González-Alfonso et al. 2010) has been shown to be able to expel the cold gas reservoir of the galaxy in about 10^7 yr (Feruglio et al. 2010).

Recently, in two notable cases (IRAS-F11119+3257 Tombesi et al. 2015 and Mrk 231 Feruglio et al. 2015), a nuclear UFO of highly-ionized gas and a galactic molecular outflow have been simultaneously observed. The energetics of these flows are consistent with a picture where energy is conserved in the wind/ISM interaction.

Finally, in the radio band outflows of neutral gas, with velocity ranging from few hundreds

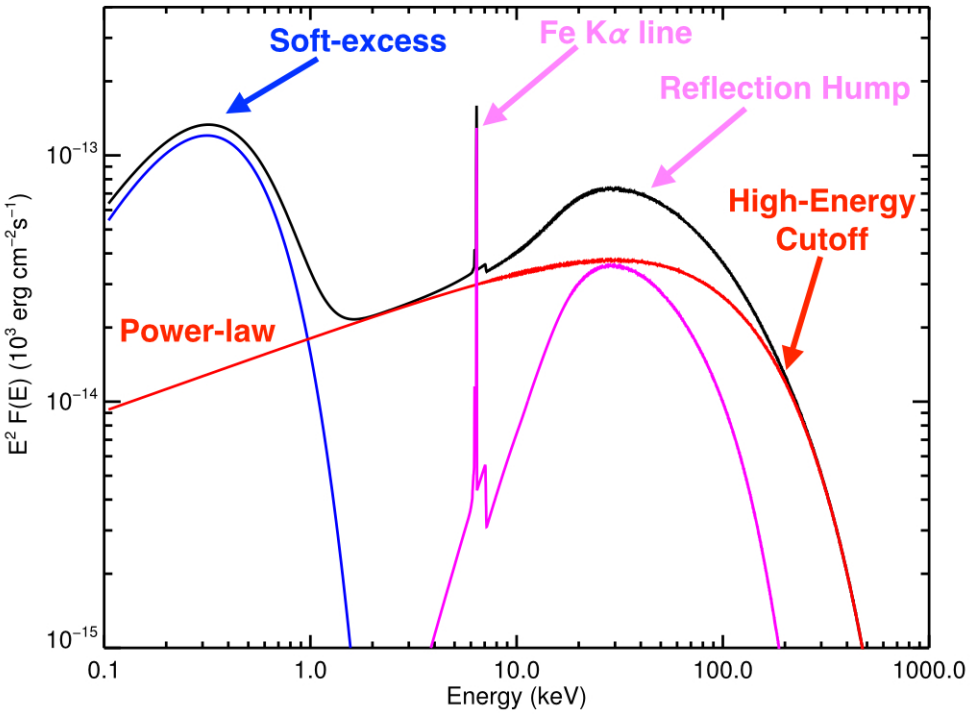

Figure I.2: Spectral components of the AGN continuum in the X-ray band. The most relevant spectral features are labeled.

up to a few thousands km s^{-1} have been discovered in a handful of radio-loud objects using the H I-line and/or the carbon monoxide (CO) transitions as tracers (see Morganti 2015, and references therein). In the best studied case (4C 12.50 Morganti et al. 2013), the Very Large Baseline Interferometer (VLBI) has imaged the H I outflow to be located off-nucleus, in a region of bright radio emission due the ongoing jet-ISM interaction. This proves that, in the case of radio-loud AGN, the activity of the jet is able to drive an outflow in the ISM of a galaxy (Wagner & Bicknell 2011, Wagner et al. 2012).

I.3 The broadband X-ray spectrum of AGN

Currently, the leading missions dedicated to X-ray astronomy are the ESA satellite X-ray Multi Mirror (XMM-*Newton*) and the *Chandra* satellite of NASA, that were both launched in 1999. Both these spacecrafts are equipped with X-ray detectors based on CCD technology (e.g., the EPIC camera Strüder et al. 2001, Turner et al. 2001 on board XMM-*Newton* and the ACIS detector on board *Chandra*), which are sensitive to X-rays in the 0.3–10.0 keV band. It is common in the terminology of X-ray astronomy to divide this bandpass

into a soft and a hard band, below and above 2.0 keV, respectively. With these non dispersive instruments, especially with the XMM EPIC-pn which has a highest effective area among the current X-ray detectors, a low-resolution (e.g., for the EPIC-pn the spectral resolving power is R=20–50) but broadband spectroscopy of astrophysical sources can be performed. This is ideal, for instance, for accessing the physics producing the AGN continuum emission. Recently, the launch of the Nuclear Spectroscopic Telescope Array (NuStar, Harrison et al. 2013), which is the first X-ray telescope capable of focusing the hard X-ray light up to ∼80 keV, has expanded the high quality coverage of X-ray band to above ∼10 keV. As we shall see important features of the AGN continuum are expected in this energy range.

I.3.1 The X-ray spectral continuum

In Fig. I.2, we show the typical X-ray spectrum of a type 1 AGN, cleaned from any absorption. This is a rather idealized case since the spectrum is often modified by absorption from both neutral and ionized gas along the line of sight. However, for clarity, we illustrate at first the spectral components of the intrinsic AGN continuum and hence in Sect. I.3.2 and in Sect. I.4 we describe the effects of cold and warm absorption on the spectrum, respectively. The knowledge of the continuum shape, especially in the soft X-ray band where most of the absorption features fall, is crucial for a correct absorption estimated. As shown in Fig. I.2, three main spectral components are typically needed to account for the X-ray continuum across the 10^{-1}–10^{3} keV band. There is a general consensus about the origin of the X-ray emission above ∼2.0 keV. In this spectral range the emission is dominated by the Comptonized radiation of the hot corona (Sect. I.1.2). The predicted power-law shaped spectrum provides a good fit for both Seyfert and quasar objects. Typical spectral slopes range between $\Gamma = 1.6-1.9$ (e.g., Bianchi et al. 2009, Piconcelli et al. 2005), with possible subtle differences between the quasar and Seyfert population. Recently, the advent of NuStar has opened the possibility of measuring the high-energy cutoff of the AGN X-ray continuum with an accuracy never achieved before (of the order of 10% in the best constrained cases, e.g., Brenneman et al. 2014, Marinucci et al. 2014a). The knowledge of both the spectral slope and of the cutoff energy allows to directly access the corona physical parameters (the temperature kT and the plasma optical depth τ).
A prominent iron line emerging over the X-ray continuum is ubiquitously detected in AGN. On average, the line peaks at the energy expected for the Kα transition of neutral iron (∼ 6.4 keV) and has an ubiquitous narrow profile (Jiménez-Bailón et al. 2005, Corral et al. 2008, Bianchi et al. 2009), which is barely resolved by current grating spectrometers (Yaqoob & Padmanabhan 2004). In some cases, a broad component (e.g., Nandra et al. 2007) can be disentangled from the narrow core. Reflection of the disk radiation in some neutral distant material (e.g., the obscuring torus, Matt et al. 1991) is a likely origin for the narrow core of the line. Conversely, the broad component may result from reflection by the disk material (Fabian 2006) or, sometimes, may be partially ascribed to the line-emitting gas in the BLR (e.g., Mrk 279, Costantini et al. 2010). For genuine disk-lines, relativistic effects may significantly affect the line profile (see Miller 2007, and references therein). Reflection processes produce also a continuum emission due to

electron scattering. The contribution of this reflected continuum to the total AGN X-ray spectrum becomes significant at hard energies. Indeed, if reflection occurs in a Compton thick material ($N_{\rm H} \geq 10^{24}$ cm^{-2}), a broad hump is expected at 30–40 keV (Murphy & Yaqoob 2009).

In the majority of type 1 AGN, the combination of a primary and a reflected continuum is not sufficient to account for the emission at energies below ∼2.0 keV. At these energies a broad excess, which can be phenomenologically modeled as a blackbody at temperatures of the order of ∼150 keV (e.g., Piconcelli et al. 2005), is often seen. This so-called soft-excess (Singh et al. 1985) cannot be ascribed to the accretion disk, because the Wien tail of the disk blackbody emission is not expected to be strong at soft X-ray energies (Sect. I.1.1).

There is no general consensus about the origin of the soft-excess. Comptonization of the disk photons in a warm, optically plasma is a viable mechanism to extend the disk emission to soft X-ray energies. The Comptonizing plasma may reside in the inner regions of the accretion disk, (Done et al. 2012) or in an extended corona located above it (Petrucci et al. 2013).

Another possible explanation invokes reflection of the primary radiation in an ionized disk (Ross & Fabian 2005). The soft X-ray spectrum of the reflected radiation would contain a wealth of fluorescence emission lines. According to this so-called light-bending model, in the case of disk reflection, the strong gravity in the vicinity of the black hole smoothen these lines in a pseudocontinuum, thereby creating the observed excess. A rapidly spinning black hole is often required in this model to justify the extreme relativistic blurring (e.g., Crummy et al. 2006).

Finally, other authors (Turner et al. 2009) have proposed that the soft X-ray spectrum of AGN is dominated by absorption in a patchy medium, which partially covers the source. As a consequence of the partial-covering, there is a leakage of flux at lower energies that modifies the continuum slope. This absorption may arise for instance in a clumpy disk wind, located within the BLR.

X-ray spectral fitting alone is not sufficient to distinguish among these models. Even in high quality dataset, (e.g., MCG 6-30-15, Ballantyne et al. 2003, Miller et al. 2008) models with drastically different physical assumptions are equally able to account for the observed spectral shape. Complementary experiments, exploiting for instance the informations contained in the time domain, may, in some cases provide a discriminating evidence. For instance, during a multiwavelength monitoring campaign of the bright Seyfert 1 Mrk 509, the UV flux followed the variability of the soft-excess (Mehdipour et al. 2011). This is easily interpreted as a Comptonization framework, where the optical/UV disk photons directly feed the Comptonizing the corona. A reflection scenario would more naturally predict a correlation between the soft-excess and the hard X-ray flux above ∼10 keV, because of the Compton reflection hump expected at ∼ 30 keV. This correlation is absent in the Mrk 509 case.

On the other hand, recent observations of short time lag between variation in the soft X-ray band with respect to the hard X-ray band (De Marco et al. 2013) have been successfully explained in a reflection based scenario (Fabian et al. 2009, Cackett et al. 2013).

I.3.2 X-ray variability

AGN are variable X-ray sources. For instance, early on it was noticed (Matt et al. 2003) that the spectra of some type 2 AGN taken at different epochs show drastic changes in both flux and spectral shape. Prompted by this finding, in the last ten years many studies have been dedicated to AGN spectral variability and a rich phenomenology has emerged. Spectral variations have been observed on timescales ranging from few hours up to few years, in both type-2 and type-1 AGN. This is often ascribed to a variable absorption of the X-ray radiation along the line of sight. For instance, on these timescales many type 2 AGN (e.g., NGC 7582, Piconcelli et al. 2007, UGC 4203, Risaliti et al. 2010, and, NGC 454 Marchese et al. 2012) have been observed to change look, switching from a Compton-thick state ($N_{\rm H} \geq 10^{24}$ cm^{-2}) to Compton thin state ($N_{\rm H} \leq 10^{24}$ cm^{-2}). Variations in the absorbing column density and/or covering fractions have been observed also in some, on average unobscured, type 1 sources. (e.g., NGC 4151, Puccetti et al. 2007, 1H 0557-385, Longinotti et al. 2009, and, SWIFT J2127.4+5654, Sanfrutos et al. 2013.) This ubiquitous rapid variability suggests that some cold X-ray absorbing material must be present in the vicinity of the central engine, even in optically unobscured AGN (Bianchi et al. 2012). This material is probably patchy and may belong to the BLR itself or to a clumpy torus extending inward beyond the dust sublimation radius (Miniutti et al. 2014).
The clumpy nature of the absorption is unambiguously witnessed by recent observations of rapid occultation and de-occultation of the X-ray source. For instance, in the best studied Seyfert 1.8 NGC 1365, a 10-hours long eclipse has been observed (Risaliti et al. 2009). Assuming a simple picture of a cloud orbiting at Keplerian velocity, the observed crossing time of the line of sight implies that the cloud is moving at $v \geq 10^4$ km s^{-1} at a distance of $\sim 10^4\, R_{\rm g}$ from the nucleus. In this scenario, the inferred physical properties of the cloud (physical size of the order of 10^{13} cm and density of 10^{10}–10^{11} cm^{-3}) are typical for the BLR material. The case of Mrk 766 (Risaliti et al. 2011) indicates that eclipsing events occur also in type 1 sources. For instance, a systematic search for eclipse events in the vast archive of AGN light curves of the Rossi X-ray timing explorer (RXTE) has encountered eight objects with multiple events (Markowitz et al. 2014).
The variable absorption can coexist with relativistic disk reflection (e.g., NGC 1365, Risaliti et al. 2013, and MCG 6-30-15 Marinucci et al. 2014b) or with a Comptonized soft-excess (e.g., NGC 5548, Mehdipour et al. 2015). In a disk reflection scenario, a variety of possible spectral appearances are predicted as the geometry of the disk-corona system changes (Miniutti & Fabian 2004). Namely, when the primary X-ray emitting spot migrates closer to the black hole, because of the stronger gravity, the radiation will be focused down to the disk, without reaching the observer. In the most extreme conditions, a low-flux, flat spectrum is predicted. For the case of e.g., Mrk 335 (Wilkins & Gallo 2015), the variable light bending may be alone sufficient to explain the spectral history of the source. In this context, in chapter 2 we test the light-bending model against a scenario based on Comptonization and variable absorption for the long-timescale variable X-ray spectrum of the bright Seyfert 1 1H 0419-477.
The analysis reported in chapter 3 of this thesis is related to the dramatic spectral changes that we witnessed in 2013, during an optical/UV/X-ray/gamma-ray observational cam-

paign dedicated to the prototypical Seyfert 1 NGC 5548. The coincidence between this historical spectral transition and our monitoring campaign provided a unique opportunity to investigate the cause of this unusual event. During the campaign, the source was ∼25 times weaker at soft X-rays than the long-term average, while behaving almost normally at energies above ∼2.0 keV. At the same time, in the UV it shows broad absorption troughs in the blue wings of e.g., the Lyα, C IV, and N V, broad emission lines, that were never present before. In Kaastra et al. (2014) we propose that all these changes are due to the onset of a weakly ionized, fast wind, located within or just outside the BLR, which blocks 90% of the soft X-ray flux in our line of sight. In chapter 3 we show that the rapid variability of this newly discovered obscurer is consistent with the picture of a patchy wind. Whether the obscuring wind in NGC 5548 is a unique case or a common mode of AGN variability is an intriguing question that deserves further investigations.

I.4 AGN ionized outflows

In the last fifteen years, thanks to advent of high resolution X-ray grating spectrometers, such as the Reflection Grating Spectrometer (RGS, den Herder et al. 2001) on board XMM-*Newton* and the low/high energy transmission grating spectrometers (LETGS, Brinkman et al. 2000, and HETGS, Canizares et al. 2005) on board *Chandra*, the field of X-ray spectroscopy has been revolutionized. With these instruments, an unprecedented spectral resolving power of R=200–1000 has become available, allowing for the first time a detailed diagnosis of the physical conditions (kinematics and ionization state) of the absorbing/emitting gas in a variety of astrophysical sources.
An advantage of X-ray spectroscopy compared to other wavelengths is that a larger bandpass is covered. Thus, numerous transitions of abundant elements such as iron, neon, oxygen, nitrogen, and carbon can be detected in a single X-ray observation. For instance, the Fe I and the O I absorption edges from a neutral gas fall in the X-ray band. X-ray transitions from ionized gas comprises a wealth of lines and edges from both lowly-ionized iron (Fe II–Fe XXIV) and oxygen (O IV–O VI), up to helium-like and hydrogen-like oxygen (O VII–O VIII), carbon (C V–C VI), nitrogen (N VI–N VII) and neon (Ne IX–Ne X). In 15 years of XMM-*Newton* and *Chandra* operations, many of these transitions have been detected both in absorption and in emission in several high resolution X-ray spectra of AGN up a redshift z of ∼0.1.

I.4.1 Warm absorber diagnostics in the X-ray and in the UV bands

A warm absorber is identified in the X-ray and in the UV spectrum of type 1 AGN via the detection of narrow absorption lines (NAL) from several ionized species of e.g., Ne, O, Fe, C, N, Mg, and Si. These lines are usually blueshifted with respect to the systemic velocity, which indicates a global outflow of absorbing gas. Transitions from low ionization species (e.g., Mg II, C II–C IV, and, Si II–Si III) are seen in the UV. Conversely, high ionization species (e.g., Ne IX–Ne X, and, O VII–O VIII) produce only X-ray features. Ions like e.g., O VI, which produces features in both bands, are suitable to investigate the connection between the

UV and the X-ray absorber.
From a single X-ray or UV spectral observation, the kinematics and the ionization conditions of the gas can in principle be estimated. However, the current UV spectrometers are sensitive to details of the velocity structure that are not resolved in the X-ray. On the other hand, determining an accurate solution for the gas ionization parameter ξ using only few UV transitions is difficult. This is not the case in the X-ray, where dozen of transitions are typically detected. For instance, the M shell transitions from many ionized iron species form a deep unresolved transition array (UTA) which is a typical feature of X-ray warm absorbers. The shape of this trough is also sensitive to small variation of the ionization parameter (Netzer 2004). For these reasons, the combination of X-ray and UV spectroscopy provides the best possible diagnostics of the physical conditions in the outflow.
In a spectral observation, the kinematics of the gas is determined straightforwardly from the Doppler shift of the absorption lines. Moreover, individual ionic column densities can be readily derived from the observed depth of the absorption lines. In the UV, a velocity dependent covering factor (Arav et al. 2002) has to be considered in the column density determination. The global properties of the absorbing gas, namely the global hydrogen column density $N_{\rm H}$ and gas ionization parameter ξ can also be accessed by fitting the numerous X-ray features with a synthetic model of a photoionized absorber (e.g., XABS, Kaastra et al. 1996). In these models the ionic column densities of different elements are linked to each other through the ionization balance prescribed by the Spectral Energy Distribution (SED) of the source. The ionization balance is computed through a photoionization code, such as Cloudy (Ferland et al. 2013) or XSTAR (Kallman 1999).
Besides characterizing the physical conditions in the outflow, the aim of the study of warm absorbers is to ascertain whether these winds are energetically important for the AGN feedback scenario. This can also be evaluated from spectroscopic observables.
According to theoretical models, the outflow can provide an effective feedback if its kinetic luminosity is comparable (i.e., between 0.5% and 5%, Hopkins & Elvis 2010, and references therein) with the AGN bolometric luminosity $L_{\rm bol}$. The kinetic luminosity is simply given by $L_{\rm kin} = \dot{M}\, v^2/2$, where v is the outflow velocity and $\dot{M}$ is the mass outflow rate. The latter scales as $\sim v\ N_{\rm H}\ r$ (e.g., Crenshaw et al. 2003b) and thus depends critically on the distance r of the outflowing gas from the nucleus.
Moreover, it depends on the geometry of the outflow, which is difficult to determine. It is often assumed (Blustin et al. 2005) that the outflow is a partially filled spherical shell of gas, with an opening angle Ω and a volume filling factor f. An average value of $\Omega = 1.6$ is derived assuming that 25% of AGN are type 1 (Maiolino & Rieke 1995) and that the covering factor of these outflows is roughly 50% (Crenshaw et al. 2003b). An analytical expression for the volume filling factor f can be derived from the prescription that the momentum of the outflow must be of the order of the momentum of the absorbed radiation plus the momentum of the scattered radiation. Namely, $\dot{M}\, v \sim \dot{P}_{\rm abs} + \dot{P}_{\rm sc} = \frac{L_{\rm abs}}{c} + \frac{L_{\rm ion}}{c}(1 - e^{-\tau_{\rm T}})$ where $L_{\rm abs}$ is the luminosity absorbed by the outflow in the 1–1000 Ry range, $L_{\rm ion}$ is the source ionizing luminosity in the same range, and $\tau_{\rm T}$ is the optical depth for Thompson scattering.
Provided that the density n of the absorber is known, the distance r can be in principle

determined from the definition of ionization parameter $\xi = L_{\rm ion}/n\,r^2$ (Tarter et al. 1969). In the UV the gas density can be in some cases directly diagnosed using some density-sensitive lines (e.g., Si II, Si III, C II, C III, and, Fe III) from collisionally-excited metastable transitions (Bautista et al. 2009).
Alternatively, the recombination timescale of a particular ion can also be used as a density indicator, as it scales like $\sim n^{-1}$. This timescale can be accessed by searching for absorption line variability in response to continuum variation and measuring the delay (or the lack of delay) in the response of a particular line. Depending on the timescales that one wants to test, this is feasible with either a single long observations (e.g., Krongold et al. 2007) or extensive monitoring campaigns (e.g., Kaastra et al. 2012). When none of these density indicators is available some milder constraints can still be put on the gas location. These are derived from some general considerations (Blustin et al. 2005). The prescription that the velocity of the outflow must be greater than the escape velocity from the black hole ($v \geq \sqrt{\frac{2GM}{c^2}}$) sets a lower limit for the distance. Conversely, an upper limit of $r \geq \frac{L_{\rm ion} f}{N_{\rm H}\,\xi}$ (where f is the volume filling factor) is derived if the thickness of the outflowing shell is not greater than its distance from the center. These constraints on the distance, although quite approximated, are in most cases sufficient for an order of magnitude evaluation of the contribution of the wind for the AGN feedback.

I.4.2 Observed properties of warm absorbers

Ionized outflows are common in AGN. About 50% (Crenshaw et al. 2003b) of radio-quiet Seyferts 1 host a warm absorber. Typical absorbing column densities range between 10^{20}–10^{23} cm^{-2}while the observed outflow velocities are of the order of few hundreds up to few thousands km s^{-1}(McKernan et al. 2007). Recently, warm absorbers analogous to those found in radio-quiet AGN have been discovered also in the X-ray spectrum of radio-loud objects (Torresi et al. 2012, and references therein). However, for radio-loud objects, the statistics of X-ray WA studied at grating resolution comprises of only four sources, including the case of 4C +74.26 that we present in Chapter 3.
In the last fifteen years UV/X-ray observational campaigns have been performed for some nearby Seyfert 1 (Costantini 2010, and references therein) unveiling the detailed structure of the outflow. Warm absorbers are multicomponents winds, covering a wide range in ionization parameter and in velocity even in the same object. The combination of X-ray and UV spectroscopy provides the complete census of the ionization and velocity components of the outflow. Hence, the interplay between the X-ray and the UV absorbing gas can be explored by comparing the gas kinematics and the ionic densities independently derived in each band.
Usually at least some of the UV and X-ray components share, within the uncertainty due to the lower X-ray spectral resolution the same kinematics (e.g., NGC 3783, Kaspi et al. 2002a, NGC 4051, Kraemer et al. 2012, and, Mrk 509, Ebrero et al. 2011). Moreover, in some cases, (e.g., Mrk 279, Arav et al. 2007) a correspondence in the ionic column densities of common ions is found, provided a covering factor acting in the UV band. These findings suggest that the UV and X-ray absorber are the manifestation of the same, composite

outflow.
Nevertheless, determining how the different gas phases are geometrically and physically related is not trivial. From the kinematical correspondence it is often inferred that the UV and the X-ray absorbing gas may be co-located (Ebrero et al. 2011). Some authors (e.g., Kraemer et al. 2012) have suggested a scenario where the UV absorbing gas is in the form of colder clumps embedded in a flow of tenuous and more highly ionized gas. This may be the case for the outflow in NGC 3783, where the high-ionization UV components have been found to have pressures similar to those of the three X-ray ionization components, (Gabel et al. 2005) which are thermally stable (Netzer et al. 2003). In other cases, the distance estimations indicate that the highly ionized components are located much closer to the black hole than lowly-ionized components (e.g., NGC 4593 Ebrero et al. 2013). This is suggestive of a stratification of the ionized matter in the wind.
The quest of measuring the density of the absorber to infer its distance has led to many studies of the WA variability on short timescales. Changes in the WA opacity or ionization were observed for instance in NGC 3783 (∼31 days, Krongold et al. 2005) and NGC 4051 (few ks–few months, Krongold et al. 2007, Steenbrugge et al. 2009). On the other hand, assessing the WA variability on long (e.g., ∼years) timescales requires that high quality multi-epoch spectroscopy is available, which is seldom the case. A multi-epoch study of the WA was attempted, for instance, in the case of Mrk 279 (Ebrero et al. 2010) without finding significant variability. A more noticeable long-term variability of the WA was observed, for instance, in Mrk 335 (Longinotti et al. 2013) where the emergence of an ionized outflow that was not historically present was observed in 2009. In this respect the WA variability that we observed during the 2013-2014 observational campaign of NGC 5548 is an outstanding case. We found that the WA has recombined in response to the dramatic lowering of the ionizing flux caused by the inner obscurer that we discovered during the campaign (Kaastra et al. 2014). Signatures of the lower-ionization WA are indeed seen in the UV and in the X-ray spectra taken during the campaign (see Arav et al. 2015 and chapter 3). In most cases, obtaining accurate estimation of the location of the absorber is not possible. Direct density indicators are rarely detected, and when available, they constrain the location only for the specific outflow component to which they belong. So far, density-sensitive lines have been detected in the UV in a handful of sources (Kraemer et al. 2006, Gabel et al. 2005, Arav et al. 2015). Attempts of measuring the gas density via the line variability have sometimes led to undetection (which implies however a robust lower limit for the distance e.g., Kaastra et al. 2014, Arav et al. 2012) or to contradictory results (Krongold et al. 2007, Steenbrugge et al. 2009, e.g., NGC 4051). Recently, Crenshaw & Kraemer (2012) have made the census of the distance estimations available so far for the well known X-ray/UV absorbers. They found that in nearby Seyferts the absorbers are located between ∼0.01 and ∼100 pc from the center, i.e., outside the BLR and inside the NLR. This range of location is consistent with a scenario where the wind originate via photoionized evaporation of matter off of the surface of the obscuring torus (Krolik & Kriss 2001).
A connection between the WA and the line emitting gas in the NLR has also been suggested in some cases (Behar et al. 2003, Detmers et al. 2009). However, accurate distance estimation of the WA and detailed multiwavelength photoionization modeling of the NLR

are needed to set a connection on a firm basis.
The kinetic luminosity carried by the warm absorber is usually modest ($\lesssim 0.1\% L_{\rm bol}$, Costantini 2010, and references therein). Thus, these ionized outflows are not expected to produce a significant feedback in the AGN environment. However, in a recent theoretical modeling of the wind/ISM interaction (Hopkins & Elvis 2010), the energy needed for an effective feedback has been found to be an order of magnitude lower ($\sim 0.5\% L_{\rm bol}$) than what was previously thought ($\sim 5\% L_{\rm bol}$). Interestingly, Crenshaw et al. (2015) have shown that the energetics of the outflow in NGC 4151, exceeds this lower benchmark if the outflow discovered in the NLR of this AGN is summed up with the classical warm absorber.

I.5 This thesis

In the cases of study treated in this thesis (1H 0419-577, NGC 5548, and, 4C +74.26) we draw a geometrical picture of the AGN gaseous environment, thanks to the analysis of the X-ray data. In each of these cases we detected an AGN outflow, with quite different characteristics.

The main results of this thesis are the following.

- In chapter 1 we analyze the longest exposed high-resolution X-ray spectrum ever taken of the Seyfert 1.5 galaxy 1H 0419-577. This was acquired as a part of a UV/X-ray campaign dedicated to this source. A simultaneous optical spectrum was also used in the analysis. We detect a thin, lowly ionized warm absorber, which is consistent to be one and the same with a galactic scale outflow detected in the UV. This is the first X-ray absorber ever detected so far away from the nucleus. Thanks to the optical/UV/X-ray spectral coverage, we could also attempt a multivawelength photoionization modeling of the narrow emission lines. The line-emitting gas is located much closer to the nucleus, at ∼pc distance. Our photoionization analysis suggests the NLR is a complex gaseous environment, stratified both in ionization and in density.
- In chapter 2 we focus on the broadband optical-to-X-ray spectrum of the same source. We successfully model it using a Comptonization model, where the disk-photons are up-scattered to X-ray wavelengths by two intervening layers of plasma having different temperatures and optical depths. The X-ray photons above ∼2.0 keV are produced in the classical hot, optically thin corona. Conversely, softer X-ray photons are produced in an another corona, which is warm and optically thick. In this framework the historical spectral variability of this source is readily explained as due to a neutral absorber with a variable opacity which intervenes in the line of sight. We speculate that the variable X-ray absorption originates in the innermost dust-free region of a clumpy torus.
- In chapter 3, we analyze several high resolution X-ray spectra that were taken in 2013-2014 in the context of a multi-satellite observational campaign of the prototypical

Seyfert 1 galaxy NGC 5548. During the campaign, we discovered the source in an unusual condition of heavy and persistent soft X-ray obscuration. We find that this newly discovered obscurer is rapidly variable, on timescale as short as two days, both in column density and in covering fraction. This is consistent with the picture of a patchy wind. In September 2013, the source underwent a two-week long re-brightening. Our analysis of the September 2013 spectrum indicates that this is a flare of the intrinsic continuum. This temporary flux enhancement provided a unique occasion to disentangle the WA features from the obscured continuum. We detect absorption from Fe-UTA, O IV-O IV, which are consistent to belong to a lower-ionized counterpart of the historical NGC 5548 warm absorber. This confirms that the WA has recombined in response to the lowering of the ionizing flux caused by the inner obscurer.

- In chapter 4, we model the X-ray absorption of the giant radio-loud quasar 4C +74.26. We clearly disentangle from the heavy Galactic absorption a highly-ionized outflow ($v \sim 3600\,\mathrm{km\,s^{-1}}$) located at the redshift of the source. This is one of the few cases so far of a well-characterized WA in a radio-loud galaxy. We discuss a scenario where the ionized gas flows along the polar axes of the source and cause an apparent redshift of the polarized Hα line. The kinetic luminosity carried by the outflowing gas is insufficient to produce a significant AGN feedback in this quasar.